IEEE Access
Multidisciplinary ⋮ Rapid Review ⋮ Open Access Journal

Received 16 July 2024, accepted 6 September 2024, date of publication 19 September 2024, date of current version 7 October 2024.

Digital Object Identifier 10.1109/ACCESS.2024.3463729

RESEARCH ARTICLE

Dielectric Modulated Charge Plasma-Based Label Free Detection of Biomolecules in Dual Metal DG TFET Biosensors

DIPSHIKA DAS[1,2], RUDRA SANKAR DHAR[1], (Senior Member, IEEE), PRADIP KUMAR GHOSH SR.[2], (Senior Member, IEEE), ARINDAM BISWAS[3,4], (Member, IEEE), SAURAV MALLIK[5,6], (Member, IEEE), NAIM AHMAD[7], AND WADE GHRIBI[7]

[1]Department of Electronics and Communication Engineering, National Institute of Technology Mizoram, Aizawl, Mizoram 796012, India
[2]Department of Electronics and Communication Engineering, Techno International New Town, Kolkata 700156, India
[3]Department of Mining Engineering, Kazi Nazrul University, Asansol, West Bengal 713340, India
[4]Centre for IoT and AI Integration, Kazi Nazrul University, Asansol, West Bengal 713340, India
[5]Department of Environmental Health, Harvard T. H. Chan School of Public Health, Boston, MA 02115, USA
[6]Department of Pharmacology and Toxicology, The University of Arizona, Tucson, AZ 85721, USA
[7]College of Computer Science, King Khalid University, Abha 62529, Saudi Arabia

Corresponding authors: Rudra Sankar Dhar (rudra.ece@nitmz.ac.in), Saurav Mallik (sauravmtech2@gmail.com), and Naim Ahmad (nagqadir@kku.edu.sa)

This work was supported in part by the Deanship of Research and Graduate Studies, King Khalid University, through the Large Research Project RGP2/404/45.

ABSTRACT In this article, we present dielectric modulation-based label free detection of biomolecules at a cavity under gate metal located near the tunneling junction of charge plasma based dual metal-double gate tunnel FET (CP-DM DGTFET). The biomolecules that settle down in the cavity act as dielectric above the tunneling junction and cause drain current to increase/ decrease. To eliminate the short channel impact and to enhance I_{ON}/I_{OFF} ratio without compromising any other device features, dual metal gate architecture with laterally split dielectric is used. The biosensor is capable of recognizing neutral, positive, and negative charges with the highest drain current sensitivity of 2.9×10^9 Ccm^{-2} and highest I_{ON}/I_{OFF} ratio of 9.02×10^{11} for biomolecule gelatin with dielectric constant $k = 12$. This work explores the effectiveness of charge-plasma based DM DGTFET for detection of biomolecules such as gelatin ($k = 12$), keratin ($k = 8$), bacteriophage T7 ($k = 6.3$), and APTES ($k = 3.57$) with varied charge distribution at various biasing. The drain current sensitivity, subthreshold slope, drain current, ON/OFF current ratio are computed for various biomolecules and their variations with respect to cavity length, biomolecule charge, etc. are used to detect unknown biomolecules. Finally, RF analysis such as gain bandwidth product, cut-off frequency, transit time, and linearity/selectivity of biosensors are incorporated. The device shows better linearity and less distortion for high –k biomolecules. The results of our studies are reproducible for repeated computed analysis.

INDEX TERMS Biosensor, charge plasma, dielectric modulation, sensitivity, split dielectric.

I. INTRODUCTION

MOSFET with nanogap has been a promising device to detect label free biomolecules. The reason behind its popularity lies in its improved detecting capacity, minimal power usage, low cost, and CMOS compatibility. Despite these benefits, FET-based biosensors have inevitable issues such as poor subthreshold swing (SS > 60 mV/dec), restricted sensitivity, elevated power dissipation caused by thermionic electron emission and short channel effects (SCEs). The technique popularly used these days is dielectric modulation [1], [2], where alterations in the gate-oxide dielectric constant (k) result in changes in the sensitivity of the biosensor. To eradicate these, researchers turned their attention to TFET that

The associate editor coordinating the review of this manuscript and approving it for publication was Paolo Crippa.

focuses on tunneling process of carriers from band to band, controlled charge transport mechanism and a steep subthreshold swing. Furthermore, label-free detection is a key feature of TFET biosensors, allowing direct observation of biomolecular interactions without requiring markers. This technique complements the device's precision charge transport management and sharp subthreshold swing by streamlining the detection procedure and increasing sensitivity. Detection and analysis of biomolecules are important for diseases diagnostic, food safety etc. Any change in concentration of some specific biomolecules may lead to malfunction of living cells. Accurate measurement of specific biomolecule concentration in living cells are very crucial to ensure optimum functioning of living organisms.

Tunnel FET based biosensors are one of the most fascinating platforms demonstrating promising potential for an electrical detection of label-free and charged biomolecules by their intrinsic charges. We have illustrated in this article how TFET based biosensors open up new possibilities for fast and on-site medical diagnostics for healthcare solutions. The analysis focuses on methodologies aiming to improving sensitivity and assessing shifts in simulated parameters such as ON current (I_{ON}), OFF current (I_{OFF}), ON-OFF current ratio (I_{ON}/I_{OFF}), Subthreshold Swing (SS), threshold voltage (V_{th}), sensitivity, and selectivity. Doping-less charge-plasma-based FET [3], [4], [5], [6] is the most popular among TFET based sensors and it also eased the process of fabrication by creating drain (N^+ region) and source (P^+ region) with appropriate work functions with respective drain and source metal contacts.

The benefits of dual metal double gate electrodes, specifically M1 (such as hafnium that forms the tunneling gate with lower work function ϕ_t to trigger the early tunneling phenomena at source-channel side) and M2 (such as aluminium that forms the auxiliary gate with higher work function $\phi_a > \phi_t$ to swipe the charges towards the drain), have also been integrated to enhance the device performance [7]. In TFETs, using a metal with a lower work function can help decrease the turn-on voltage. This happens because a smaller work function enhances the bending of the energy bands at the source-channel interface, which promotes more efficient electron tunneling and improves performance at lower voltages. While a metal gate having higher work function at the drain-channel junction reduces the OFF current by increasing the energy barrier, which limits electron leakage when the device is in the OFF state. Also, this leads to a decrease in ambipolarity behaviour, hindrance of short channel effects, and reduced drain-induced barrier lowering (DIBL). Girish et al [8] proposed dual metal charge plasma TFET (DM CPTFET) biosensor with a hetero gate structure. For various dielectrics, they conducted sensitivity analysis. Dibyendu et al [9] found superior sensitivity performances of hetero dielectric as compared to single dielectric. Utilizing low-k dielectric closer to the drain and high-k dielectric close to the source [10], [11] as well as better gate modulation at the channel-source intersecting tunnel junction would help reduce ambipolar conduction. To enhance the ON and OFF state electrostatics, high-k spacers have been explored for optimization of digital and analog performance [12], [13]. Recent research show that subthreshold swing (SS) is more improved where ferroelectric material is used as gate dielectric [14], [15], [16]. Some architectures employ diagonal tunneling, providing superior junction electrostatics and gate control [17] while some architectures implement both vertical and lateral tunneling [18]. Recently, using chalcogenide thin films in graphene-based Surface Plasmon Resonance (SPR) sensors has shown enhanced sensitivity and precision in detecting biomolecular interactions. Different ranges of doping techniques in junctionless devices [19] and placement of biomolecules with respect to tunneling junction [20] have proved significant impact for various detectability parameters of biomolecules. It has become evident that the sensitivity of biosensors depends on cavity length [21], [22], [23], drain doping, gate underlap/ overlap [24], multigate configuration [25], additional/extended cavity region [26], [27], [28], additional core gate [29], different gate shapes [30], [31] and biomolecule charge types [32]. The heterojunction TFET architecture [33], [34], [35] shows the suppression of ambipolar conduction and outperform in analog/DC operations. The effect of gate electrode length and metal electrode work function variation has been analyzed in for improving band-to-band tunneling efficiency [11]. In the context of detecting biomolecules, the studies of some parameters such as limit of detection (LOD), limit of quantification (LOQ), linearity, sensitivity, selectivity and reproducibility are very crucial. LOD refers to the minimum concentration of a biomolecule that can be reliably distinguished and are calculated using standard deviation of the response curve and the slope of the calibration curve. LOQ is the same as the LOD if predefined objectives are met. For the reliable and fast detection, it is expected that the characteristic parameters should show linear variation with respect to the concentration of analytes such as biomolecules. Linearity limit defines the operating range between the LOQ and the point where the plot goes non-linear. The correctness of the observation is decided by the term reproducibility which shows the ability of the biosensor to produce identical responses for a repeated experimental setup. This parameter of the sensor is characterized by the accuracy and precision of the associated electronics circuits.

In this proposed structure, a nanocavity has been created under the M1 gate electrode to detect biomolecules like proteins, amino acids, etc. DNA molecules with polarization and the ability of dipole movements act as both negative and positive charge can also be detected by using the sensor in a high end bioengineering laboratory. This structure offers improved sensitivity for neutral and charged biomolecules. The variation in electrical characteristics, namely, drain current I_d, I_{ON}/I_{OFF} ratio, sensitivity and device efficiency are captured to identify biomolecules with different dielectric values and charge density. To avoid capacitive coupling of gate over the tunneling junction, an opening close to gate is used that acts as inlet to the biomolecules towards the cavity. The device's performance is evaluated using the Silvaco ALTAS device simulator.

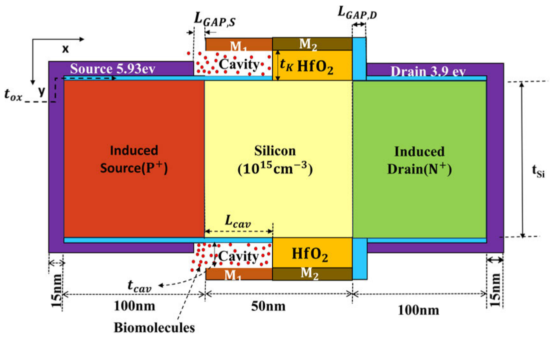

FIGURE 1. Cross-section of dielectric modulated charge plasma based DM DGTFET.

II. DESIGN OF SENSOR

Fig. 1 presents the cross-sectional view of the dielectric modulated charge plasma-based dual metal double gate TFET. The parameters of the device include a single Silicon layer (t_{Si}) of 10 nm thick with intrinsic carrier concentration $n_i = 10^{15}$ cm^{-3}, channel length $L_T = 50$ nm, with different metal work functions above the channel. In this charge plasma-based structure, the drain and source are developed by surrounding the regions with the optimum work function of 3.9 eV and 5.93 eV, respectively [7], [37]. Considering the compliance with Debye's length for optimal performance that avoids quantum effects, a 10 nm silicon body thickness (t_{Si}) is used.

In Charge Plasma based DM DGTFET, two different dielectrics are used as the gate dielectric. The tentative process flow of the given biosensor with a nanogap cavity using standard IC fabrication techniques is illustrated in Figure 2 and elaborated as follows: (1) Initially, an intrinsic (100) silicon wafer with a substrate thickness of 10 nm is considered. (2) A layer of HfO2 is deposited at the gate region cavity using atomic layer chemical vapor deposition with high K and then patterned using chemical mechanical planarization (CMP). (3) An atomic layer of SiO_2 (0.5 nm) is formed on the silicon surface through precise oxidation exposure. (4) Dummy oxidation is performed to shield the cavity and spacer regions at the source end from metal deposition. (5) Certain sections of the insulator are eliminated away using dry etching. (6) Metallization is carried out using a lower-function metal to provide the source electrode, drain electrode, and gate region. (7) Additional metals from the spacer are etched to provide insulation from gates. (8) Selective regions (source electrode, auxiliary gate metal) are exposed to an annealing process with the desired metal gas to achieve different work functions. (9) The sacrificial layer deposited at the cavity and inlet regions is etched away to create the cavity region. (10) Two identical wafers are joined together using the wafer bonding technique to provide dual cavity regions. (11) The bonded wafer forms the desired biosensor device.

Table 1 depicts the permittivity of various biomolecules under study along with the source of references. The dual metal gate allows higher electrostatic capacity to regulate the channel by enabling alignment of the energy bands. Based on the IRDS 2022 roadmap, 0.5 nm SiO_2 equivalent oxide thickness (EOT) is employed below the cavity under tunneling gate and a high-k dielectric (HfO_2) is employed under the auxiliary gate. The region below the tunnel gate metal and above the 0.5 nm SiO_2 layer forms the cavity that acts as trapping site for targeted biomolecules [38]. Due to the differences in physical thickness of laterally split dielectrics, a cavity structure is created below the tunneling gate. The cavity is surrounded by source electrode (work function 5.93 eV) on its left, high-k dielectric (HfO_2) on the right, tunnel gate metal M1 on the top and 0.5 nm SiO_2 layer on the bottom. As soon as biomolecules build up within the cavity, an overall dielectric constant at channel-source intersecting region changes which results in energy band bending and ensures onset of the tunneling phenomena.

TABLE 1. Biomolecules with respective dielectric constants.

Biomolecules	DIELECTRIC CONSTANT (K)
APTES	3.57[38]
Bacteriophage T7	6.3[39]
Keratin	8[40]
Gelatin	12[41]

The cavity capacitance C_{cav} is given by

$$\text{Ccav} = \frac{\varepsilon_{SiO_2} * k}{k * t_{ox} + \varepsilon_{SiO_2} t_{cav}} \quad (1)$$

where ε_{SiO2} and k are the permittivity of SiO_2 layer, and the biomolecule, respectively, t_{ox} being the thickness of SiO_2 layer. Here fully filled cavity is considered for investigation with the cavity dimensions (length, L_{cav} and thickness, t_{cav}). The cavity under study has the dimensions of 20 nm × 2.7 nm. The influence of cavity dimensions on the ability to sense biomolecules is being investigated here. The calculation is repeated for other dimensions of cavity 12 nm ×2.5 nm. Here fully filled cavity is considered for investigation with the cavity dimensions (length, L_{cav} and thickness, t_{cav}). The cavity under study has the dimensions of 20 nm × 2.7 nm. The influence of cavity dimensions on the ability to sense biomolecules is being investigated here. The calculation is repeated for other dimensions of cavity 12 nm ×2.5 nm. The immobilization of biomolecules is facilitated by a 3 nm gap ($L_{GAP,S}$) between gate and source electrodes. The spacer width between the gate and drain electrode ($L_{GAP,D}$) has been optimized [43], [44] and is inserted with 15 nm thick layer of SiO_2 layer. The tunneling gate is placed over the cavity, as pointed out in Fig. 2. Table 2 gives the device specification of the given structure. Here fully filled cavity is considered for investigation with the cavity dimensions (length, L_{cav} and thickness, t_{cav}). The 2D simulator named Silvaco ATLAS is used to aid the simulation of CP DM DGTFET [45].

TABLE 2. Device parameters specification.

Specification	Symbol	Parameter values
Length of total gate region, nm	L_T	50
Length of cavity region, nm	L_{cav}	20
Thickness of cavity region, nm	t_{cav}	2.7
Tunnel gate work-function, eV	ϕ_t	3.9
Auxiliary gate work-function, eV	ϕ_a	4.5
Spacer thickness, nm	$L_{GAP,S}$, $L_{GAP,D}$	3, 15
SiO_2 thickness, Å	t_{ox}	5
High dielectric thickness, EOT	t_k	0.5

The distinct models considered are the bandgap narrowing, Auger models, non-local band-to-band tunneling model, Fermi–Dirac statistics Lombardi (CVT) model, band-to-band quantum tunneling, Shockley–Read–Hall (for recombination) and field-dependent mobility model. To study the way, it performs in the OFF-state, the simulation also incorporates the trap-assisted tunneling model. Moreover, to evaluate the numerical tunneling probability Wentzel-Kramers-Brillouin (WKB) technique is employed.

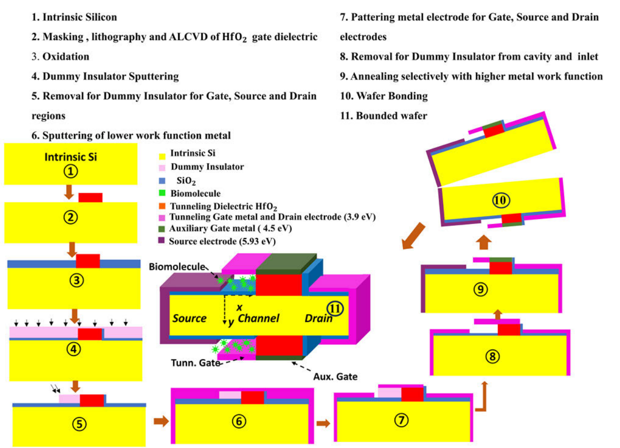

FIGURE 2. Proposal of fabrication flow diagram for dielectric modulated charge plasma based DM DGTFET.

The models and characteristics of the reported work [46] are also used to demonstrate the viability of the simulator in the suggested model. To validate the simulator, the drain characteristics are extracted from the reported paper using the plot digitizer tool. When the cavity is filled with air, the transfer characteristics of calibrated biosensor almost match the reported result, as exhibited in Fig. 3.

III. RESULTS AND DISCUSSION

When biomolecules are positioned into the cavity, the gate capacitance alters the interactions between the channel and the gate electrodes through electrostatic interaction. It perturbs various electrical characteristics like I_{ON}/I_{OFF} ratio,

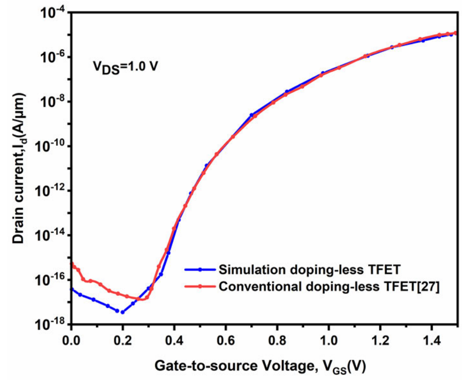

FIGURE 3. Drain current calibration of CP DM DGTFET biosensor compared with reported research work [46] at fixed V_{DS} = 0.1 V.

subthreshold swing (SS), transfer characteristics, and energy band bending. In this section, minimum tunneling phenomena is noted for air filled cavity (k = 1) and is used throughout the literature to act as a constant reference value.

A. EFFECT OF k AND CHARGE OF BIOMOLECULES ON ENERGY BAND DIAGRAMS

The source - channel junction has a wide potential barrier width in the OFF state (V_{DS} = 0.5 V and V_{GS} = 0 V) as noticed in Fig.4(a). The valence band of the source and the conduction band of the channel are not aligned in the OFF state (the dotted lines). Solid lines represent the energy band diagram in the ON state (V_{DS} = 0.5 V and V_{GS} = +1.5 V). Due to the narrow tunneling barrier in this state, electrons engage in tunneling, and transition from the conduction band of the channel to the valence band of the source. The results are obtained for a positive charge biomolecule with dielectric constant k = 12 for a fixed cavity length of 20 nm. Fig. 4(b) shows a band diagram response for the ON and OFF state conditions for a positive and a negative charged biomolecule in the cavity with a constant relative permittivity k = 5 for a cavity length of 20 nm. The graph clearly shows that the positive charge biomolecule shifts the energy band downwards, while negative biomolecules shift the energy band upwards.

For the positive charge biomolecules, gate capacitance has more electrostatic control over intrinsic channel thus enhancing early commencement of tunneling phenomena. On the other hand, a fully filled cavity with negative charged biomolecules results in gentle misalignment of energy bands thus reducing tunneling phenomena at ON state and consequently drain current drops down.

B. EFFECT OF CAVITY LENGTH ON DRAIN CURRENT

The drain characteristics of CP DM DGTFET for the neutral biomolecule with a fixed relative permittivity k = 6.3 for different cavity length are shown in Fig.5(a). It is noticed that for cavity length greater than 10 nm, the dependency of length of cavity on drain characteristics is not significantly pronounced. This is due to the presence of an effective work

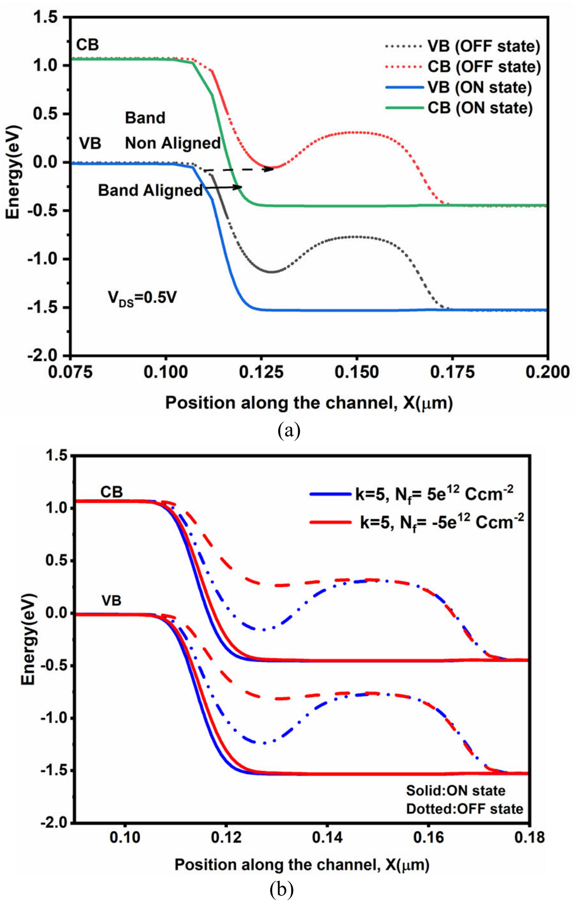

FIGURE 4. **Band diagram for energy during the ON and OFF state conditions (a) Effect of the neutral biomolecule dielectric constant k = 12. (b) Comparison of energy bands for biomolecules with negative and positive charges for the same dielectric constant k = 5.**

function metal over the junction area between the channel and the source. It is sufficient to trigger lateral tunneling. For reduced cavity length of 6 nm or less, the channel offers more resistance to tunneling current until it attains threshold voltage (which is 1.1 V). This is due to reduced covering area of lower work function metal. To prevail the tunneling phenomena, one requires larger area of lower metal work function of gate ϕ_t to increase the steepness at the tunneling junction. The I_{OFF} remains the same due to reduced ambipolarity behaviour owing to dual metal structure of gate. For higher cavity length $L_{cav} = 25$ nm, the ambipolarity behaviour is found significantly less and so less band bending at channel-drain region eventually lower the I_{OFF} effectively. Hence the optimum choice of cavity length is taken as $L_{cav} = 20$ nm for further investigation.

With fixed $L_{cav} = 20$ nm, $V_{DS} = 0.5$ V, drain characteristics with regard to a variety of biomolecules are plotted in Fig. 5(b) for the given structure. When a biomolecule of different dielectric constant (from Table 1) enters the cavity region, the energy barrier between the source and the channel narrows down, and hence I_{ON} rises. The biomolecules here act as a modulating parameter for controlling tunneling

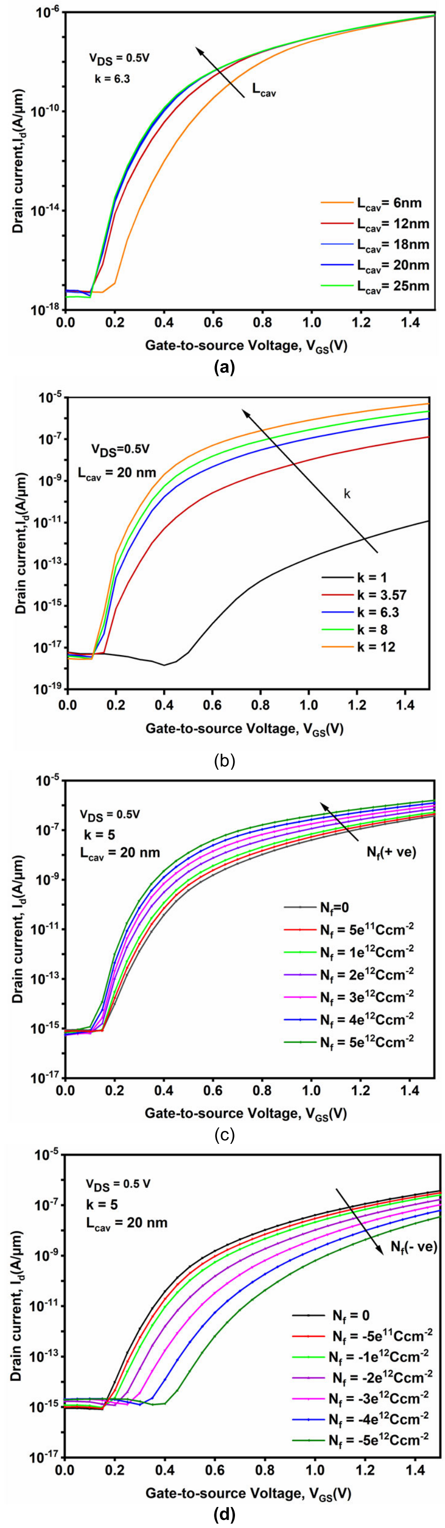

FIGURE 5. **Transfer characteristics of CP DM DGTFET with a fixed V_{DS})=0.5 V (a) Cavity length, L_{cav} = 6, 12, 18, 20 and 25 nm (b) Dielectric constant (k = 1, 3.57, 6.3, 8, and 12) (c) Positive charge distribution (ranging from 0 Ccm^{-2} to 5 × 10^{-12} Ccm^{-2}) for k = 5. (d) Negative charge distribution (ranging from 0 Ccm^{-2} to - 5 × 10^{-12} Ccm^{-2}) for k = 5.**

electrons from source to channel. As relative permittivity of neutral biomolecule increases, the electrostatic coupling of gate voltage over lateral tunneling point increases, resulting I_{ON} to increase as shown in Fig. 5(b). The suggested structure can therefore identify biomolecules that have been calibrated against dielectric constant.

For positively charged biomolecules immobilized in the cavity with fixed $V_{DS} = 0.5$ V and fixed $k = 5$, drain current variation is plotted in Fig. 5(c) for a fixed cavity length of $L_{cav} = 20$ nm. It has been noted that increased positive charge strengthens the tunneling phenomenon and hence raises the drain current. On the other hand, I_{OFF} remains unchanged as the channel-drain junction remains unaffected. For the similar reason, negative charged biomolecule reduces I_{ON} with increased negativity due to widening of tunneling barrier as depicted in Fig. 5(d).

C. EFFECT OF k ON DRAIN SENSITIVITY AND SELECTIVITY

Drain sensitivity is a crucial factor to detect various biomolecules. The drain sensitivity may be defined as the ratio of the drain current $I_{d(Bio)}$ when the cavity is completely occupied with biomolecules to the drain current $I_{d(air)}$ when it is vacant or occupied with air). Thus.

$$\text{Drain Sensitivity} = \frac{\text{Id(Bio)}}{\text{Id(air)}} \tag{2}$$

The drain sensitivity is studied for a fixed V_{DS} =0.5 V and with varying gate voltage, charge, cavity length and dielectric. The drain sensitivity is larger for positively charged biomolecules, as shown in Fig. 6(a). Higher positive charge molecules enhance the early onset of tunneling phenomena. The peak drain sensitivity increases from 6.5×10^7 to 1.3×10^9 as the charge distribution increases from neutral to 5×10^{12} Ccm^{-2}. Fig. 6(b) shows negative charge molecules reducing the tunneling phenomena by inducing gentle slope at the tunneling junction. Our studies reveal that the drain sensitivity shows a wide variation from 6.5×10^7 to 4.46×10^3 as the negativity of biomolecule changes from neutral to -5×10^{12} Ccm^{-2}. Hence, we conclude that the designed device is able to identify the presence and type of charge of biomolecules in a cavity. This is explained by the fact that the charges affect coupling of gate with the silicon channel and shifts energy band upside/ downside at the source- channel transition region for positive/ negative charges, respectively. In Fig. 6(c), we study drain sensitivity against various cavity lengths, and it shows that for longer cavity, the drain sensitivity is good enough to detect biomolecule while shorter cavity length results in shorter tunneling gate length hence lesser impact to enhance the ON current of the sensor. For cavity length 20 nm and 25 nm the results have been studied for neutral biomolecule with $k = 6.3$ and drain sensitivity is found to be almost the same. We discussed earlier that the energy band of the channel region drops down and the gate control effectiveness of the device becomes stronger for high-dielectric biomolecules. As evident from Fig.6(d), for k =12, the highest drain current sensitivity attained is 2.9×10^9. Therefore, the tunneling probability function between the source and the channel is increased, and hence offers higher drain current, and consequently greater drain sensitivity as shown in Fig. 6(d).

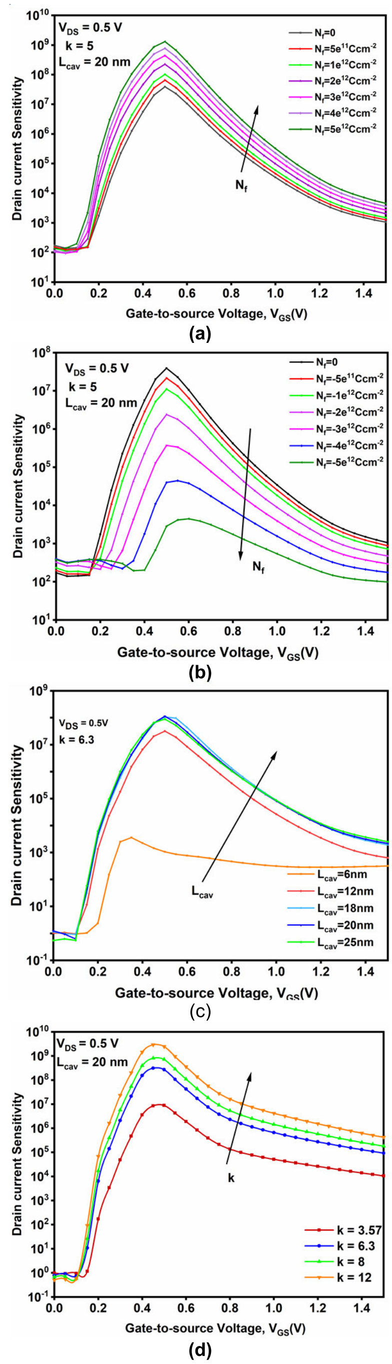

FIGURE 6. **Show the plot of drain sensitivity at fixed $V_{DS} = 0.5$ V with variation of (a) Density of positive charges (which ranges from 0 Ccm-2 to 5×10^{-12} Ccm^{-2} for fixed relative permittivity k = 5 and $L_{cav} = 20$ nm. (b) Density of negative charges (which ranges from 0 Ccm^{-2} to -5×10^{-12} Ccm^{-2} for fixed relative permittivity k = 5, $L_{cav} = 20$ nm (c) Cavity length (L_{cav} = 6, 12, 18, 20, 25 nm) for neutral biomolecule with k = 6.3 (d) Relative permittivity of various neutral biomolecules (k = 3.57, 6.3, 8, 12) for $L_{cav} = 20$ nm.**

Identifying a particular biomolecule from many other biomolecules is accomplished in terms of the parameter

"Selectivity" (ΔS) which is defined as under.

$$\Delta S = \frac{I_d(k2) - I_d(k1)}{I_d(k1)} \tag{3}$$

where k2, k1 are biomolecules of different dielectrics.

In our work, distinguishability of keratin ($k = 8$), from bacteriophage T7 ($k = 6.3$) can be obtained as

$$\Delta S_1 = \frac{I_d(k=8) - I_d(k=6.3)}{I_d(k=6.3)} = 1.27083.$$

Similarly, for the pair gelatin and keratin the selectivity is calculated as $\Delta S_2 = \frac{I_d(k=12)-I_d(k=8)}{I_d(k=8)} = 22.21$.

With the presented architecture, specific biomolecule binding happens through the cavity approach, which uses a label-free sensing technique based on dielectric modulation. This ensures that the amount of the targeted analyte is properly transduced to a proportionate modification of the output electric signals. A complete study of selectivity can be obtained by transient analysis of the device.

D. EFFECTS ON SUBTHRESHOLDSWING

The influence of neutral biomolecules on subthreshold swing (SS) is shown in the bar plot of Fig. 7 for given structure of cavity length $L_{cav} = 20$ nm. When the relative permittivity of neutral biomolecules is varied from $k = 3.57$ to 12, it shows variation from 28 mV/dec to 17 mV/dec, while air-filled cavity shows a SS of 70 mV/dec. The decrease in SS with dielectric constant is due to feeble effect of dielectric on tunneling junction for enhancing tunneling current, while dual metal work function enables the device to switch from ON to OFF state in a faster way. The minimum SS achieved for the device at $k = 12$ is 17 mV/dec. As evident from Fig. 7, this device performs well at a low supply voltage ($V_{DS} = 0.5$ V).

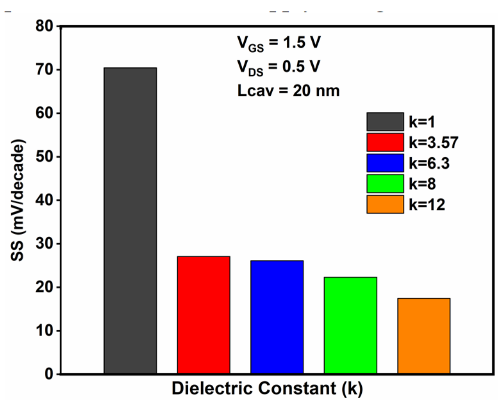

FIGURE 7. Subthreshold slope (SS) for various neutral biomolecules at $V_{GS} = 1.5$ V, $V_{DS} = 0.5$ V and $L_{cav} = 20$ nm.

E. EFFECTS ON AVSS AND I_{ON}/I_{OFF}

The average subthreshold slope(AVSS) is defined as

$$AVSS = \frac{V_t - V_{off}}{\log(I_d(V_t) - I_d(V_{off}))} \tag{4}$$

where V_t is threshold voltage of the tunnel FET and V_{off} is the voltage V_{GS} when device is in OFF state. The drain current $I_d(V_{off})$ refers to the case when the device is OFF and $I_d(V_t)$ corresponds to the current at the threshold voltage. The effect of neutral biomolecules on AVSS have been studied and the result is plotted in Fig.8. (a). Similar to the explanation given in Fig. 6 (d), when dielectric constant (k) of neutral biomolecules increases, the I_{ON}/I_{OFF} ratio rises because I_{ON} increases without any change in the I_{OFF}. Also, it shows that when the dielectric constant gets higher, the average SS within the cavity falls. It is observed from Fig. 8 (a) that the I_{ON}/I_{OFF} ratio increases with higher k–values of the biomolecules due to the reasons explained earlier. Additionally, it is noted in Fig. 8 (a) that the AVSS decreases rapidly for k less than 4. A smaller SS obtained from this biosensor dictates a better electrical response and an easy ability of detection.

For charged biomolecules, the I_{ON}/I_{OFF} ratio and average subthreshold slope (AVSS) is plotted in Fig. 8(b) with respect to the variation of charges from negative to positive. At tunneling junction, as the positive value of charge increases, the I_{ON} current is enhanced due to steep band bending of energy bands. Consequently, the current ratio and AVSS increases.

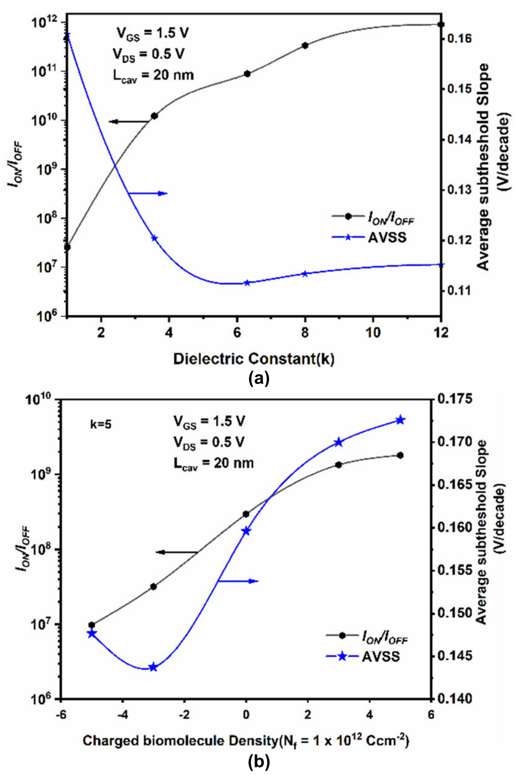

FIGURE 8. Variation of AVSS, and I_{ON}/I_{OFF} ratio of Charge Plasma based DM DGTFET for (a) Neutral biomolecules for $L_{cav} = 20$ nm (b) Charged molecules of constant permittivity $k = 5$ and $L_{cav} = 20$ nm.

F. EFFECT OF k ON SURFACE POTENTIAL

Investigating the surface potential beneath the nanogap cavity is vital to grasping the electrostatic potential behaviour of the charge plasma-based DM DGTFET biosensor. The surface potential along the channel corresponding to different dielectric constants is illustrated in Fig. 9(a). It is shown that when biomolecules are absent (k =1), the surface potential is lowest. The reason for this is that a higher dielectric constant causes a stronger coupling between the gate and the channel, which in turn causes the barrier width at the source–channel interface to decrease. This effectively raises the surface potential, for k > 1. Examining the nano system channel region, one observes contour waves of electrostatic potential based on the movement of carriers which begins at the source and ends at the drain as shown in Fig. 9(b). The presence of neutral biomolecules creates strong potential contours in the cavity region, thereby influencing the tunneling of holes in the source-channel interface. This is due to the additional influence of dielectric of the biomolecules.

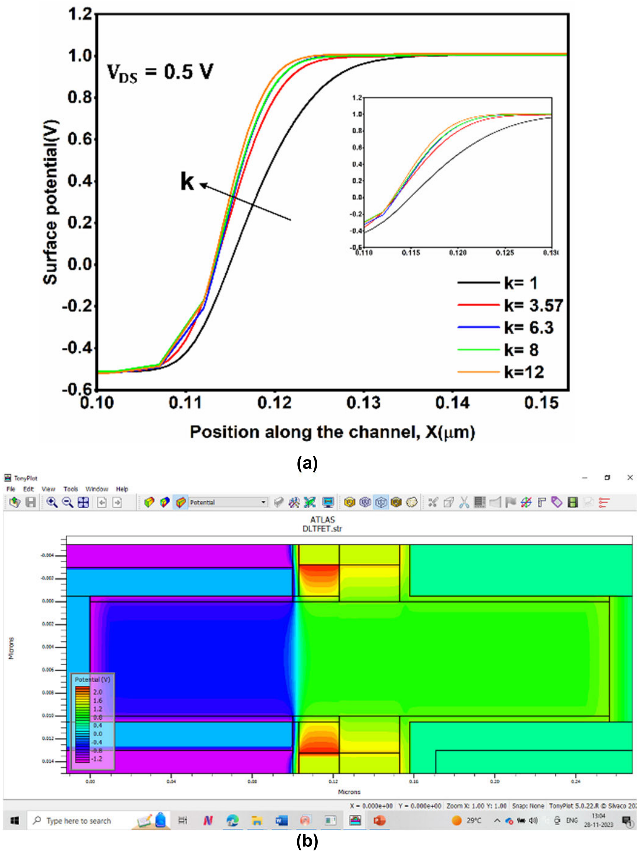

FIGURE 9. **(a) Surface potential along the channel for various biomolecules at constant V_{DS} = 0.5 V. (b) Electrostatic potential contours observed across the channel at constant V_{DS} = 0.5 V, V_{GS} = 1.5 V, and for k = 12.**

G. EFFECTS OF k AND CHARGES ON DEVICE EFFICIENCY

Another pertinent parameter that can measure the device's capability to convert drain current I_d into g_m, is the device efficiency, $\left|\frac{g_m}{I_d}\right|$. Here, gm denotes the transconductance of a device and is given as

$$g_m = \left.\frac{dI_d}{dV_{GS}}\right|_{V_{DS=Constant}} \tag{5}$$

A rise in the maximum value of $|g_m/I_d|_{max}$ is the feature that most clearly distinguishes distinct biomolecules. The spatial shifts in subthreshold swing and $|g_m/I_d|_{max}$ is of different magnitudes for different biomolecules.

The effect of device efficiency $|g_m/I_d|$ as a sensing metric for the suggested biosensor is depicted in Figures. 10(a-e). It is established that as biomolecules build up, capacitance between the gate and the channel rises. Hence it improves the electric field, which may then be used to regulate the energy bands to enable carrier tunneling and drain current. It is evident in Fig. 10 (a-d), that at lower drain current, the transconductance to the current ratio (g_m/I_d) is comparatively higher because the presence of biomolecules eventually overcoming the tunneling barrier. After attaining higher gate voltage (V_{GS} < 1 V), as the transconductance decreases, drain current saturates, hence negative differential resistance (NDR) and negative differential transconductance (NDT) are observed in Fig. 10 (a). The quantum mechanical phenomena, NDT reflects the change of g_m from positive to negative values. In the absence of biomolecules (i.e. filled with air) the onset of tunneling phenomena could not be possible hence the controlling of drain current reduces. Gate architecture is maintained with fixed EOT throughout, but the presence of biomolecules at source-channel interface modulates NDT, thus enabling to recognize different biomolecules. Positively charged molecules, for the same reason, show a higher $|g_m/I_d|_{max}$ at the lower drain current Fig. 10(b). It would be easier to detect different biomolecules by knowing the shift in the maximum device efficiency at constant current values. Similarly, for negative biomolecules, the device efficiency decreases almost proportionally, as shown in Fig. 10(c).

Fig. 10(d) shows the variation of device efficiency with drain current for different cavity lengths. Higher cavity lengths, increases the tunneling gate length. Thus, with low drain current, the electric field at the source - channel interface promotes the start of tunneling. An optimized device structure with neutral biomolecules (k = 6.3) is thus found with a cavity length of 20 nm. For higher dielectric biomolecules, one can observe the tunneling phenomena predominates at lower drain current and operating V_{GS} as |gm/Id |max shifts leftwards as shown in Fig.10(e). In Fig. 10(e), the plot of device efficiency against V_{GS} is shown. It emphasizes that neutral molecules with k = 3.57, 6.3, 8, and 12, achieve $|g_m/I_d|_{max}$ at V_{GS} equals 0.15 V approximately. At lower voltages, the tunneling switches from OFF to ON state.

H. EFFECTS OF k ON ELECTRIC FIELD AND BAND TO BAND TUNELING (BTBT) RATE

Figure 11 illustrates the electric field profile for various neutral biomolecules. It has been noted that when biomolecules' dielectric properties increase, so does the electric field. This occurs when the suggested device gate voltage is 1.5 V for k = 12, as discussed in Fig. 10(e). When there is no biomolecule present in the cavity, an electric field of around 1.17 MV/cm is produced; when gelatin is present, a maximum electric field of around 1.96 MV/cm grows up across

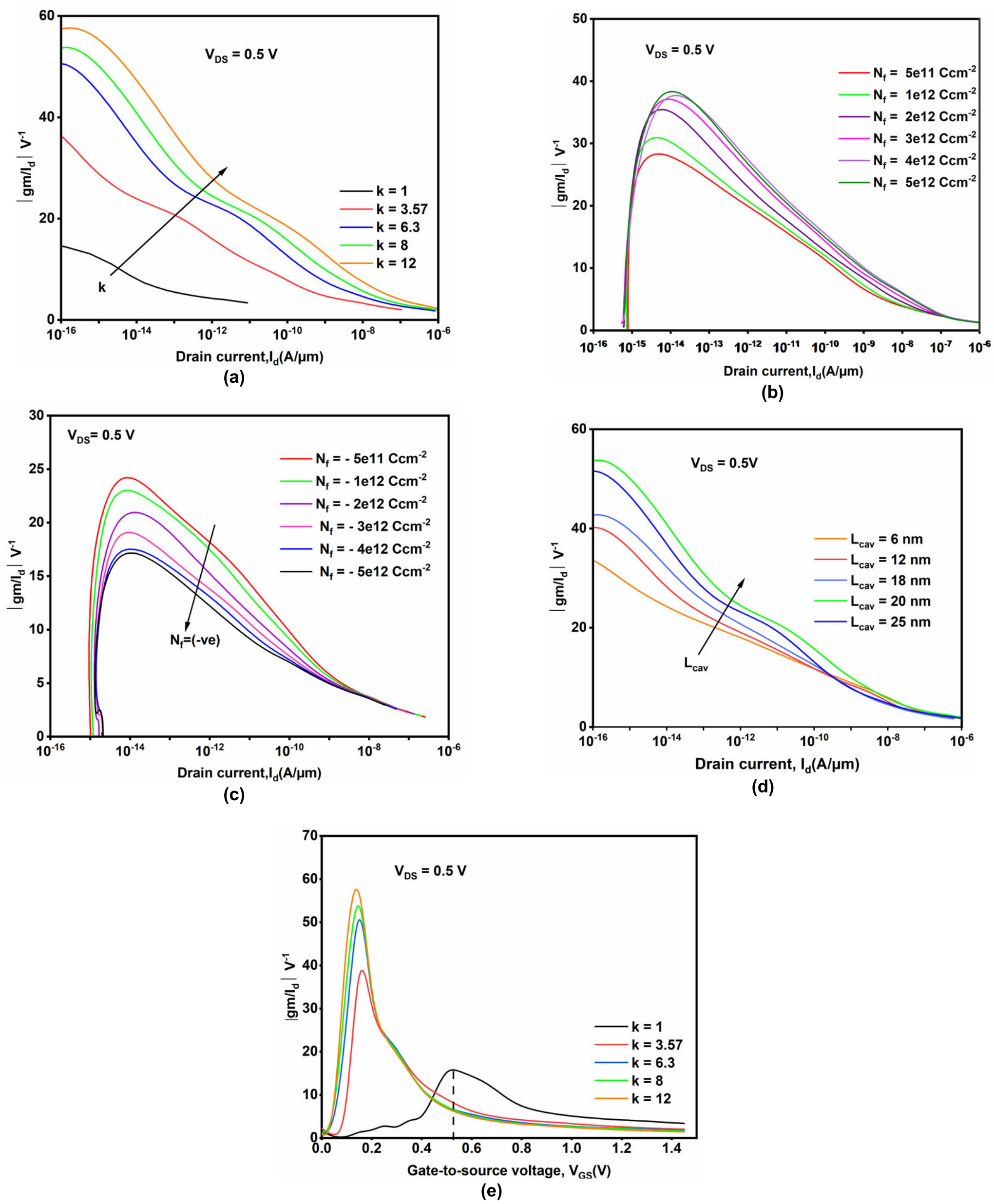

FIGURE 10. Device efficiency $|g_m/I_d|$ at $V_{DS} = 0.5$ V with variation of (a) I_d for neutral biomolecule (b) I_d for positive charge biomolecule (c) I_d for negative charge biomolecule (d) I_d for cavity length variation (e) V_{GS} for different neutral biomolecule.

the channel. The higher the value of k, the narrower is the bell-shaped response just above the cavity due to additional electrostatic control at the junction.

The band to band tunneling rate (BTBT) for different biomolecules is shown in Fig. 12. The electron tunneling rate rises with the dielectric values. This behaviour can be explained in the light of high capacitive coupling for higher k-values that lead to more energy band alignment favoring high tunneling.

I. RADIO-FREQUENCY ANALYSIS

The evaluation of the radio frequency (RF) performances of the given structure for various biomolecules is also provided, as it is vital for maintaining low dynamic power consumption. The characteristics of gain bandwidth product (GBP), transconductance (g_m), gate-to-drain capacitance (C_{gd}), and cut-off frequency (f_T) are measured in this work. The capability to convert the given gate voltage into drain current is defined by the parameter transconductance (g_m).

Gate-to-drain capacitance (C_{gd}) is a parasitic capacitance in the devices, crucial for radio-frequency applications. Analyzing C_{gd} is essential to study switching behaviour and power dissipation of the device in circuits. It is defined by

$$C_{gd} = \frac{\partial Q_g}{\partial V_{DS}} \tag{6}$$

where Q_g is the charge on gate.

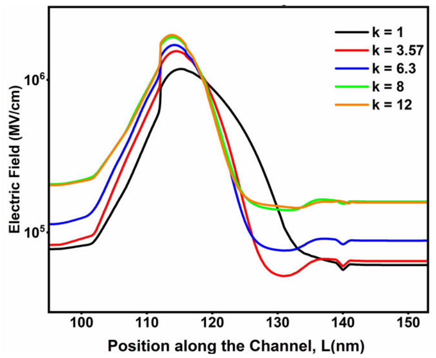

FIGURE 11. Variation of electric field observed across the channel at constant $V_{DS} = 0.5$ V, $V_{GS} = 1.5$ V.

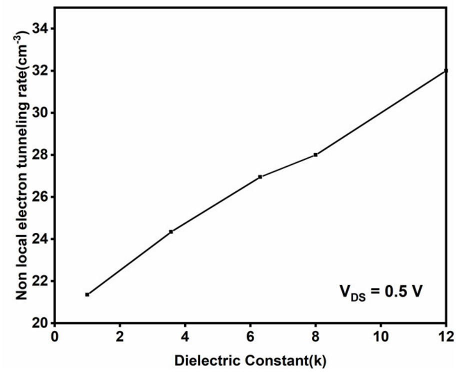

FIGURE 12. Electron tunneling rate for different biomolecules at constant VDS = 0.5 V, and VGS = 1.5 V.

Figure 13(a) shows that transconductance with the neutral biomolecules increases with the dielectric constants; g_m shows almost linear dependence with gate voltage for all k- values for, $V_{GS} > 0.7$ V. The variation of C_{gd} with gate voltage for various biomolecules has been plotted in Fig. 13(b) and indicates that an increase in dielectric results in a reduction of capacitive coupling at channel-drain region. This is due to the lower density of states, making it favorable for high-frequency regime. The charge builds up at the drain junction; hence, the total parasitic capacitance increases with gate voltage.

At a voltage close to 0.7 V, there is a rapid increase in g_m. The cut-off frequency (f_T), which denotes the device can act as a unity-gain current amplifier is a further aspect for quicker switching applications. It is given by

$$f_T = \frac{g_m}{2\pi C_{gg}} \tag{7}$$

where $C_{gg} = C_{gs}+C_{gd}$, and C_{gs} is the depletion capacitances source with respect to gate. Fig. 13(c) demonstrates the variation of f_T for neutral biomolecules in the cavity. Induction of tunneling at source – channel region due to the high-k dielectric materials results in higher cut off frequency. Near linear increase in cut off frequency with the gate voltage (>0.7V) can be explained in the light of nature

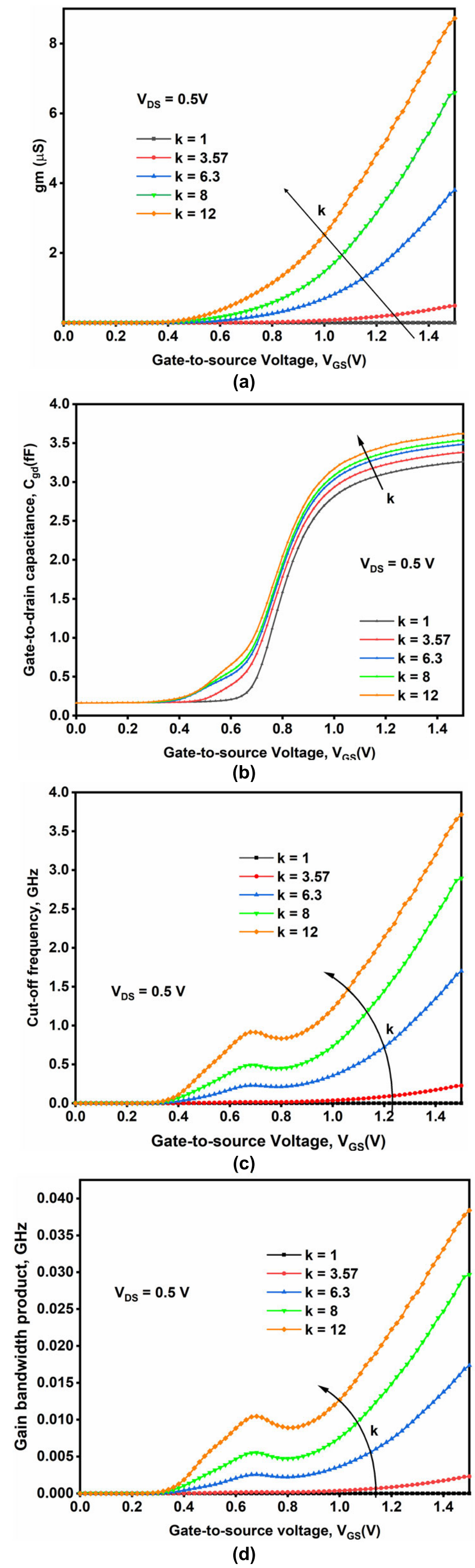

FIGURE 13. RF analysis with constant $V_{DS} = 0.5$ V (a) g_m (b) C_{gd} (c) f_T (d) GBP for various neutral biomolecule.

of variation of C_{gd} of Fig. 13(b). As g_m continues increasing more steeply for CPTFET, and parasitic capacitance builds up at the channel- drain region till $V_{GS} = 1$ V, the f_T going on increasing linearly as expected. In absence of biomolecule (k = 1), there is large tunnel gap at source junction, hence feeble possibility of tunneling of hole. Thus, increase in cut off frequency to be utilized for detection of biomolecules.

The gain bandwidth product has similar behaviour as f_T as plotted in Fig. 13(d). It is the product of bandwidth and gain, and it represents the device's working region over its steady gain region. It is used in the high frequency region and is expressed as

$$GBP = \frac{g_m}{20\pi C_{gd}} \tag{8}$$

Another metric for studying high-speed operation is the transit time (t_t). The duration required for charge carriers to traverse the channel region is referred to as the transit time (t_t) and can be expressed as follows:

$$t_t = \frac{1}{2\pi f_T} \tag{9}$$

A shorter transit time leads to faster operation of the transistor, contributing to improved switching speeds and overall device performance. The transit times (t_t) for distinct neutral biomolecules are shown in Figure 14. The device shows higher sensing speed for high k dielectric biomolecules like gelatin. Charges swipe through the channel; hence higher dielectric induces narrowing of tunneling barrier with increase in the gate voltage.

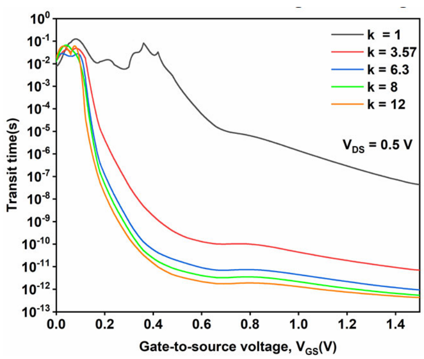

FIGURE 14. Variation of t_t with V_{GS} for various neutral biomolecules at constant $V_{DS} = 0.5$ V.

J. LINEARITY ANALYSIS

Minimal signal distortion is crucial for maintaining the integrity and quality of the signal as far as the high-frequency transport of carriers is concerned. Hence linearity analysis has been carried to investigate its performance while working in radio frequency regime. The device linearity is studied here for various biomolecules in term of the parameters such as voltage intercept point(VIP), Input intercept point(IIP), and Intermodulation Distortion(IMD), as defined below:

$$g_{mn} = \frac{1}{n!}\frac{\delta^n I_d}{\delta V_{GS}^n} \tag{10}$$

$$VIP2 = 4\left(\frac{g_{m1}}{g_{m2}}\right) \tag{11}$$

$$VIP3 = \sqrt{24 \times \left(\frac{g_{m1}}{g_{m3}}\right)} \tag{12}$$

$$IIP3 = \frac{2}{3} \times \left(\frac{g_{m1}}{g_{m3} \times R_s}\right) \tag{13}$$

$$IMD3 = \left[\frac{9}{2} \times (VIP3)^2 \times g_{m3}\right]^2 \times R_s \tag{14}$$

where transconductance is represented as gm, and 'n' denotes the order which can be n=1, 2, 3…and the value of R_s is usually taken as 50 Ω for RF application. Second-order distortion (proportional to g_{m2}) generates harmonics and intermodulation products at twice the input frequency, causing cross-modulation. Third-order distortion (proportional to g_{m3}) creates in-band intermodulation products, leading to significant interference within the system's bandwidth. For any device, higher-order parameters such as VIP2, VIP3 and IIP3 should be large as possible for achieving linearity with respect to various DC parameters. The plot of VIP2, VIP3 and IIP3 with respect gate to source voltage for various biomolecules at fixed bias of $V_{DS} = 0.5$V are shown in Figure 15(a), (b) and (c), respectively. Biomolecules with higher k shows more linearity metrics, as depicted in Fig.15(a). With a high k biomolecule, the tunneling is more and g_m attains a constant value thus providing more linear response. The metric VIP3 is more important as it involves gm of third order. VIP3 for various biomolecules, with k=1, 3.57, 6.3, 8 and 12 are plotted in fig 15(b). VIP3 with air-filled cavity(k=1) is shown in subplot (i) of Fig.15(b) and so on. The variation of VIP3 with respect to the applied gate bias shows peaks occurring at different bias voltage for different biomolecules. When the cavity is filled with high-k biomolecule, the device shows less distortion. Another way to asses this nonlinearity is the measure of IIP3 as shown in Fig.15(c). It is obvious that the peaks are observed beyond saturation for all the studied biomolecules.

The variation of IMD3 with input gate voltage is shown in figure 15(d). It affirms that the device is poorly effected from non-linearity while detecting biomolecules. Lower the value of IMD3, the less is the effect of nonlinearity.

The drain current values obtained by the present devices for different biomolecules are compared with the previously reported biosensor works [1], [7], [14], [15], [38] in Table 3. The values of the published works are acquired and are compared with the neutral biomolecule present in the cavity of the present devices. The biosensor exhibits enriched sensitivity than other charged biomolecules at lower operating voltages instigating the fact that the present biosensor devices designed here are much healthier providing enhanced performances.

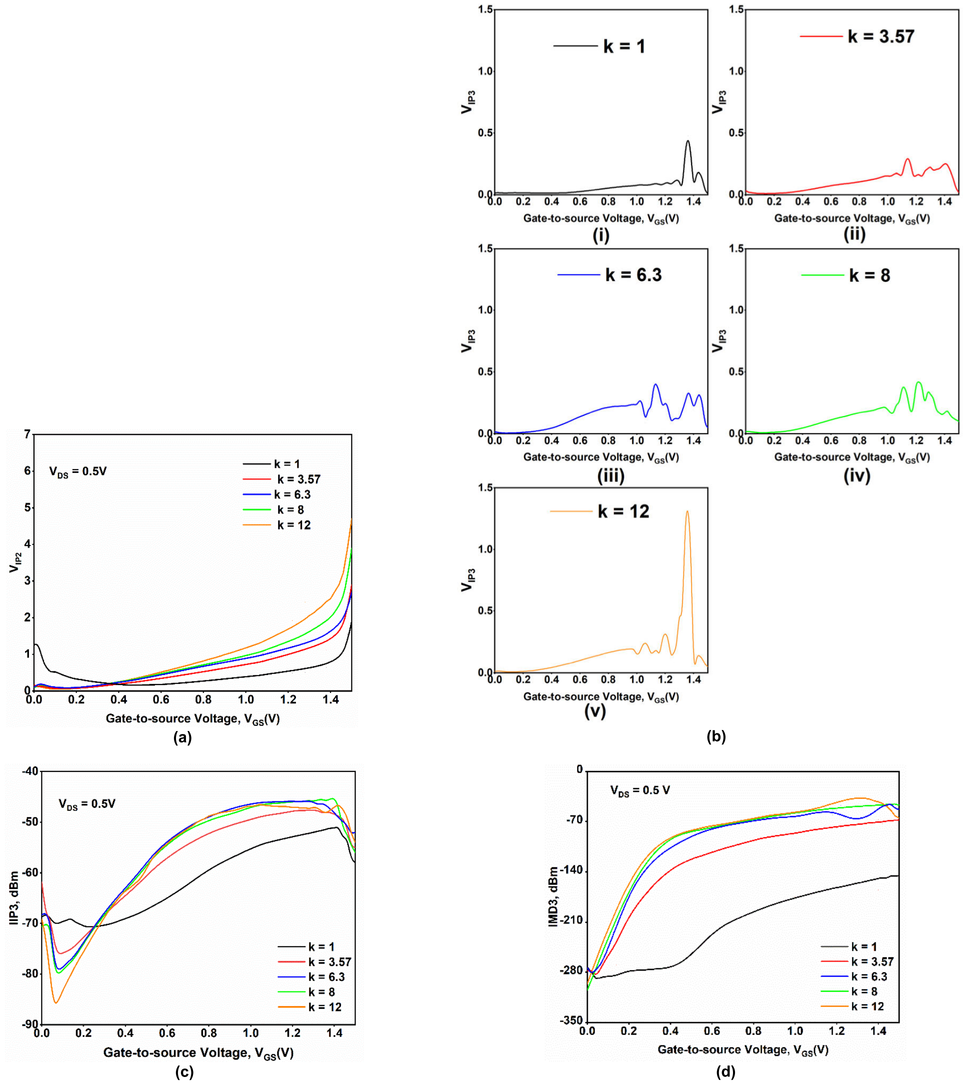

FIGURE 15. Variation of (a) VIP2, (b)VIP3, (c) IIP3 and (d) IMD3 with constant V_{DS} = 0.5 V for various neutral biomolecules.

TABLE 3. Comparison of fet-based biosensor performance with previously reported works.

	Targeted Biomolecules (K values)	Present work	Reported works
Drain Current (A/μm) at (V_{GS} = 1.5 V) & (V_{DS} = 1 V)	Neutral 3.57	1.00×10^{-6}	5.11562×10^{-9} [37]
	Neutral 6.3	5.13×10^{-6}	2.01×10^{-7} [37]
	Neutral 8	1.17×10^{-5}	9.17×10^{-7} [37]
	Neutral 12	2.43×10^{-5}	5.31801×10^{-6} [37]
			4.00374×10^{-6} [1]
I_{ON}/I_{OFF} ratio at (V_{GS} : 1.5 V) & (V_{DS} : 1 V)	Neutral 12	9.02×10^{11}	8.09×10^{11} [37]
			1.45×10^{8} [14]
			3.77×10^{9} [15]
Subthreshold Swing (SS)	Neutral 12	17mv/dec	21.7 mV/dec [37]
Drain current (A/μm) at (V_{GS} : 1.2 V) & (V_{DS}: 1 V)	k = 6.3	4.99×10^{-6}	3.9×10^{8} [15]
	k = 12	2.13×10^{-5}	3.76×10^{-8} [15]
Drain current (A/μm) at (V_{GS} : 1.2 V) & (V_{DS} : 0.5 V)	k = 8	3.54×10^{-6}	2.20×10^{-7} [7]
	k = 12	8.02×10^{-6}	9×10^{-7} [7]

IV. CONCLUSION

A charge plasma-based DM DGTFET for the detection of label-free biomolecules has been explored and analyzed using dielectric modulation in the cavity beneath the tunnel gate metal. Electrostatic features like energy band diagram, drain characteristics, drain current sensitivity, subthreshold swing, and RF performance have been investigated for the biosensor. The energy band diagram in the ON and OFF state conditions for the device is explored for both neutral, positive, and negative charge biomolecules. A detailed investigation reveals that lower cavity lengths (∼ 6 nm) require a higher gate voltage to achieve drain current than higher cavity lengths (> 12 nm). Drain current saturates at higher V_{GS} for all cavity dimensions, and with the optimal cavity length at 20 nm, drain sensitivity is at its maximum. The highest drain current sensitivity of 1.3×10^9 is attained for positive charge biomolecules and 2.9×10^9 for neutral biomolecules (k = 12). Notably, the peak of the drain sensitivity shows a wide variation with respect to the charges of the biomolecules. Also the cavity length has profound impact on the drain current sensitivity. The study shows that the subthreshold swing (SS) decreases for higher k, showing a maximum of 70 mV/dec for an air-filled (k = 1) cavity sensor. The I_{ON}/I_{OFF} ratio increases with both k and charges of biomolecules since I_{ON} increases without significant change in I_{OFF}. Here, a proper calibration has led to the detection of the charge on the biomolecule over the range between -5×10^{12} to 5×10^{12}Ccm^{-2}. AVSS also decreases negative charge densities of biomolecules. So, a variation of AVSS with k suggests easy detection of biomolecules in the sensor.

The channel electric field profile is bell-shaped as usual; a high k narrows down the profile, establishing strong electrostatic control on the charge transport in the channel. Also, the band-to-band tunneling rate is higher for higher k. The sensor's RF performance is evaluated, and it is found that both gm and C_{gd} increase with $V_{GS}(> 0.4$ V) and dielectric constant k, as expected. The cut-off frequency f_T increases almost linearly with the gate voltage (> 0.7 V), as does the gain bandwidth product. To distinguish biomolecules from others, metric selectivity is defined and discussed. Finally, the linearity analysis for the device is investigated by studying the higher orders of VIP, IIP, and IMD. The device becomes more linear and stable for biomolecules with high k values. The RF analysis covers the transit time, cutoff frequency, and gain bandwidth product and shows that the device is faster for detecting neutral and charged biomolecules. With robust electrostatic control, enhanced tunneling rates, and favorable RF performance metrics, the split-dielectric CP DM DGTFET emerges as a promising solution for biosensing applications.

ACKNOWLEDGMENT

The authors extend their appreciation to the Deanship of Research and Graduate Studies at King Khalid University for funding this work through Large Research Project under grant number RGP2/404/45.

REFERENCES

[1] S. Anand, A. Singh, S. I. Amin, and A. S. Thool, "Design and performance analysis of dielectrically modulated doping-less tunnel FET-based label free biosensor," *IEEE Sensors J.*, vol. 19, no. 12, pp. 4369–4374, Jun. 2019.

[2] S. Yadav, A. Gedam, and S. Tirkey, "A dielectric modulated biosensor for SARS-CoV-2," *IEEE Sensors J.*, vol. 21, no. 13, pp. 14483–14490, Jul. 2021.

[3] N. K. Singh, D. Mandal, and R. Kar, "Design of charge-plasma-based cylindrical-gate-nanowire TFET with low power and enhanced sensitivity for bio-sensing," *Appl. Phys. A, Solids Surf.*, vol. 127, no. 5, pp. 1–9, Apr. 2021.

[4] D. Manaswi, S. R. Karumuri, and G. Wadhwa, "Design and parametric analysis of charge plasma junctionless TFET for biosensor applications," *IEEE Open J. Nanotechnol.*, vol. 4, pp. 71–76, 2023.

[5] D. Manaswi and K. S. Rao, "Design and analysis of DGDMJL TFET for biosensing applications," *Silicon*, vol. 15, no. 14, pp. 5947–5961, May 2023.

[6] B. Dewan, S. Chaudhary, D. Singh, and M. Yadav, "A physics-based model of dielectric modulated TFET biosensor considering non-ideal hybridization issue," *Micro Nanostruct.*, vol. 183, Nov. 2023, Art. no. 207668.

[7] B. Dewan, S. Chaudhary, and M. Yadav, "A label-free dielectric-modulated biosensor using SiGe-heterojunction dual cavity dual metal electrically doped TFET," *Eng. Res. Exp.*, vol. 5, no. 3, Jul. 2023, Art. no. 035002.

[8] G. Wadhwa and B. Raj, "Label free detection of biomolecules using charge-plasma-based gate underlap dielectric modulated junctionless TFET," *J. Electron. Mater.*, vol. 47, no. 8, pp. 4683–4693, May 2018.

[9] D. Chowdhury, B. P. De, B. Appasani, N. K. Singh, R. Kar, D. Mandal, N. Bizon, and P. Thounthong, "A novel dielectric modulated gate-stack double-gate metal-oxide-semiconductor field-effect transistor-based sensor for detecting biomolecules," *Sensors*, vol. 23, no. 6, p. 2953, Mar. 2023.

[10] R. Narang, K. V. S. Reddy, M. Saxena, R. S. Gupta, and M. Gupta, "A dielectric-modulated tunnel-FET-based biosensor for label-free detection: Analytical modeling study and sensitivity analysis," *IEEE Trans. Electron Devices*, vol. 59, no. 10, pp. 2809–2817, Oct. 2012.

[11] D. Das, R. S. Dhar, and P. K. Ghosh, "Performance evaluation of split high-K material based stacked hetero-dielectrics tunnel FET," *Phys. Scripta*, vol. 98, no. 12, Nov. 2023, Art. no. 124002.

[12] M. A. Raushan, N. Alam, M. W. Akram, and M. J. Siddiqui, "Impact of asymmetric dual-k spacers on tunnel field effect transistors," *J. Comput. Electron.*, vol. 17, no. 2, pp. 756–765, Feb. 2018.

[13] A. Pon, A. Bhattacharyya, B. Padmanaban, and R. Ramesh, "Optimization of the geometry of a charge plasma double-gate junctionless transistor for improved RF stability," *J. Comput. Electron.*, vol. 18, no. 3, pp. 906–917, Apr. 2019.

[14] S. Singh, S. Singh, M. K. A. Mohammed, and G. Wadhwa, "Dual cavity dielectric modulated ferroelectric charge plasma tunnel FET as biosensor: For enhanced sensitivity," *IEEE Trans. Nanobiosci.*, vol. 22, no. 1, pp. 182–191, Jan. 2023.

[15] S. Singh, S. Singh, M. K. A. Mohammed, K. Kishor Jha, and S. A. Loan, "Reliability and sensitivity analysis of double inverted-T nano-cavity label-free Si:HfO_2 ferroelectric junctionless TFET biosensors," *RSC Adv.*, vol. 12, no. 42, pp. 27179–27188, Sep. 2022.

[16] O. Paul, C. Rajan, D. P. Samajdar, T. Hidouri, and S. Nasr, "Ge/GaAs based negative capacitance tunnel FET biosensor: Proposal and sensitivity analysis," *Silicon*, vol. 14, no. 16, pp. 10475–10483, Mar. 2022.

[17] S. J. Mukhopadhyay, B. Majumdar, K. N. Chappanda, S. C. Mukhopadhyay, and S. Kanungo, "Performance analysis of the diagonal tunneling-based dielectrically modulated tunnel FET for biosensing applications," *IEEE Sensors J.*, vol. 21, no. 19, pp. 21643–21652, Oct. 2021.

[18] N. N. Reddy and D. K. Panda, "Performance analysis of Z-shaped gate dielectric modulated (DM) tunnel field-effect transistor-(TFET) based biosensor with extended horizontal N+ pocket," *Int. J. Numer. Model., Electron. Netw., Devices Fields*, vol. 34, no. 6, p. e2908, May 2021.

[19] A. Biswas, C. Rajan, and D. P. Samajdar, "Sensitivity analysis of physically doped, charge plasma and electrically doped TFET biosensors," *Silicon*, vol. 14, no. 12, pp. 6895–6908, Oct. 2021.

[20] R. Goswami and B. Bhowmick, "Comparative analyses of circular gate TFET and heterojunction TFET for dielectric-modulated label-free biosensing," *IEEE Sensors J.*, vol. 19, no. 21, pp. 9600–9609, Nov. 2019.

[21] G. Wadhwa, P. Kamboj, J. Singh, and B. Raj, "Design and investigation of junctionless DGTFET for biological molecule recognition," *Trans. Electr. Electron. Mater.*, vol. 22, no. 3, pp. 282–289, Jun. 2021.

[22] P. Vimala, L. L. Krishna, and S. S. Sharma, "TFET biosensor simulation and analysis for various biomolecules," *Silicon*, vol. 14, no. 13, pp. 7933–7938, Jan. 2022.

[23] P. Raut, D. K. Panda, U. Nanda, and C.-C. Hsu, "Simulation and modeling of high-sensitive JL-TFET based biosensor for label free detection of biomolecules," *Microsyst. Technol.*, May 2024, doi: 10.1007/s00542-024-05638-7.

[24] D. B. Abdi and M. J. Kumar, "Dielectric modulated overlapping gate-on-drain tunnel-FET as a label-free biosensor," *Superlattices Microstructures*, vol. 86, pp. 198–202, Oct. 2015.

[25] S. Choudhury, K. L. Baishnab, K. Guha, Z. Jakšić, O. Jakšić, and J. Iannacci, "Modeling and simulation of a TFET-based label-free biosensor with enhanced sensitivity," *Chemosensors*, vol. 11, no. 5, p. 312, May 2023.

[26] R. Paul, "Simulation and performance evaluation of charge plasma based dual pocket biosensor using SiGe-heterojunction TFET design," *Silicon*, vol. 15, no. 5, pp. 2147–2162, Oct. 2022.
[27] A. Gedam, B. Acharya, and G. P. Mishra, "Design and performance assessment of dielectrically modulated nanotube TFET biosensor," *IEEE Sensors J.*, vol. 21, no. 15, pp. 16761–16769, Aug. 2021.
[28] D. Soni, D. Sharma, M. Aslam, and S. Yadav, "Approach for the improvement of sensitivity and sensing speed of TFET-based biosensor by using plasma formation concept," *Micro Nano Lett.*, vol. 13, no. 12, pp. 1728–1733, Dec. 2018.
[29] A. Gedam, B. Acharya, and G. P. Mishra, "Junction optimization of the geometry of a charge plasma double gate junctionless transistor for improved RF stabilityless silicon nanotube TFET for improved DC and radio frequency performance," *Silicon*, vol. 13, no. 1, pp. 167–178, Feb. 2020.
[30] K. A. Abdulquyyaum, S. Tiwari, R. Saha, and S. Hoque, "Sensitivity extraction of step shape double gate (SSDG) TFET biosensor considering non-ideal scenario," *Eng. Res. Exp.*, vol. 5, no. 3, Aug. 2023, Art. no. 035049.
[31] N. N. Reddy, P. Raut, and D. K. Panda, "GSE and GWE techniques to improve on (ION) current and ambipolar conduction of tunnel FET(TFET) device: A comprehensive review," *Micro Nanostruct.*, vol. 191, Jul. 2024, Art. no. 207865.
[32] S. Das and B. Sharma, "Gate-on-drain overlapped L-shaped channel tunnel FET as label-free biosensor," *Silicon*, vol. 14, no. 9, pp. 4899–4905, Jul. 2021.
[33] J. Batakala, R. Sankar Dhar, K. Kumar, A. Biswas, S. Mallik, N. Ahmad, W. Ghribi, and A. Said Badawy, "Exploration and analysis of temperature and performance of compound semiconductor-based junctionless GAA FET," *IEEE Access*, vol. 12, pp. 66910–66920, 2024.
[34] K. N. Priyadarshani, S. Singh, and A. Naugarhiya, "Dual metal double gate Ge-pocket TFET (DMG-DG-Ge-pocket TFET) with hetero dielectric: DC & analog performance projections," *Silicon*, vol. 14, no. 4, pp. 1593–1604, Feb. 2021.
[35] B. Dewan, S. Chaudhary, and M. Yadav, "A charge plasma based label free biomolecule detector using SiGe-heterojunction double gate tunnel FET," *Silicon*, vol. 14, no. 7, pp. 3259–3268, 2021.
[36] M. Tornow, "Biomolecules in electric fields," in *Encyclopedia of Applied Electrochemistry*. Berlin, Germany: Springer, 2014, pp. 132–135.
[37] G. Wadhwa and B. Raj, "Parametric variation analysis of symmetric double gate charge plasma JLTFET for biosensor application," *IEEE Sensors J.*, vol. 18, no. 15, pp. 6070–6077, Aug. 2018.
[38] M. Patil, A. Gedam, and G. P. Mishra, "Performance assessment of a cavity on source ChargePlasmaTFET-based biosensor," *IEEE Sensors J.*, vol. 21, no. 3, pp. 2526–2532, Feb. 2021.
[39] E. Makarona, E. Kapetanakis, D. M. Velessiotis, A. Douvas, P. Argitis, P. Normand, T. Gotszalk, M. Woszczyna, and N. Glezos, "Vertical devices of self-assembled hybrid organic/inorganic monolayers based on tungsten polyoxometalates," *Microelectronic Eng.*, vol. 85, nos. 5–6, pp. 1399–1402, May 2008.
[40] A. Cuervo, P. D. Dans, J. L. Carrascosa, M. Orozco, G. Gomila, and L. Fumagalli, "Direct measurement of the dielectric polarization properties of DNA," *Proc. Nat. Acad. Sci. USA*, vol. 111, no. 35, pp. 3624–3630, Aug. 2014.
[41] T. Z. Rizvi and M. A. Khan, "Temperature-dependent dielectric properties of slightly hydrated horn keratin," *Int. J. Biol. Macromolecules*, vol. 42, no. 3, pp. 292–297, Apr. 2008.
[42] P. Raut, U. Nanda, and D. K. Panda, "Analytical drain current model development of twin gate TFET in subthreshold and super threshold regions," *Microelectron. J.*, vol. 135, May 2023, Art. no. 105761.
[43] D. S. Yadav, D. Sharma, S. Tirkey, D. G. Sharma, S. Bajpai, D. Soni, S. Yadav, M. Aslam, and N. Sharma, "Hetero-material CPTFET with high-frequency and linearity analysis for ultra-low power applications," *Micro Nano Lett.*, vol. 13, no. 11, pp. 1609–1614, Nov. 2018.
[44] A. Chauhan, G. Saini, and P. K. Yerur, "Improving the performance of dual-k spacer underlap double gate TFET," *Superlatt. Microstruct.*, vol. 124, pp. 79–91, Dec. 2018.
[45] *ATLAS Device Simulation Software*, Silvaco Int., Santa Clara, CA, USA, 2016.
[46] M. J. Kumar and S. Janardhanan, "Doping-less tunnel field effect transistor: Design and investigation," *IEEE Trans. Electron Devices*, vol. 60, no. 10, pp. 3285–3290, Oct. 2013.

DIPSHIKA DAS received the B.Tech. degree in electronics and communication from the Hooghly Engineering & Technology College, in 2009, and the M.Tech. degree in electronics and communication engineering from Techno India, Salt Lake, in 2011. She is currently pursuing the Ph.D. degree in electronics and communication engineering with the National Institute of Technology, Mizoram, India. Since 2011, she has been an Assistant Professor with the Electronics and Communication Engineering Department, Techno International New Town, Kolkata, India. Her research interests include the design and simulation of dual material dual gate tunnel field effect transistor and its application.

RUDRA SANKAR DHAR (Senior Member, IEEE) received the B.E. degree from CVRCE, Utkal University, India, in 2002, the master's degree in microelectronics engineering from the University of Newcastle, U.K., in 2006, and the Ph.D. degree in nanotechnology engineering from the University of Waterloo, Canada. He was a Postdoctoral Fellow with the University of Alberta, Canada. He has also more than 20 years teaching and research experience at some of the reputed industry and institutes globally, such as Chipworks Inc., Canada, and Nanyang Technological University, Singapore. Since December 2015, he has been with the Department of ECE, NIT Mizoram, India. He is currently the Dean Academics of NIT Mizoram and had been the Founding HoD of the Centre of Interdisciplinary Research in the Institute. He is also the Ex-Head of the Department of Electronics and Communication Engineering, NIT Mizoram. He is the author of three books, twelve granted patents, and more than 130 articles in international peer-reviewed journals and conferences. His research interests include semiconductor device physics, nanomaterials technology, bioelectronics and sensor devices, renewable hybrid and green energy design, solar photovoltaics, microelectronics, applications for 1D, 2D, and 3D quantum structures. He is a Reviewer of many reputed journals, such as IEEE TRANSACTIONS ON NANOTECHNOLOGY and *RSC Advances* and an editor of many Scopus indexed journals and conference proceedings. He is an elected fellow and a Life Member of IETE and IEI. He received the Best Teacher's Award 2022 in Engineering at NIT Mizoram and the best paper award in different international conferences. He has organized and chaired many international conferences in India and abroad.

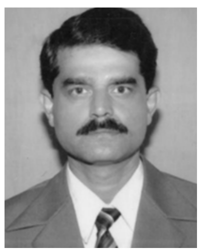

PRADIP KUMAR GHOSH SR. (Senior Member, IEEE) received the B.Sc. degree (Hons.) in physics and the B.Tech., M.Tech., and Ph.D. (Tech.) degrees in radio physics and electronics from Calcutta University, in 1986, 1989, 1991, and 1997, respectively. To his credit, he has more than 115 technical research papers in journals of international/national repute and conference proceedings in the fields of semiconductor devices, wireless communications, and signal processing. He is currently a Professor with the Department of ECE, Techno International New Town, Kolkata. He is a reviewer of many international journals. He has supervised six research scholars for the award of Ph.D. degrees. He has authored several books on digital communications, probability theories & stochastic process, and error correcting codes, published from national and international publishers. His current research interest includes tunnel FET devices. He is a Life Member of Indian Society for Technical Education (ISTE), New Delhi.

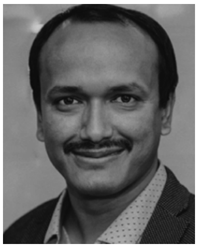

ARINDAM BISWAS (Member, IEEE) received the M.Tech. degree in radio physics and electronics from the University of Calcutta, India, in 2010, and the Ph.D. degree from NIT Durgapur, in 2013. He was a Postdoctoral Researcher with Pusan National University, South Korea, with the prestigious BK21PLUS Fellowship, South Korea. He was a DST-JSPS Invitation Fellow with RIE, Japan; a DST-ASEAN Invitation Fellow with Duy Tan University, Vietnam, and Taylors University, Malaysia; and a Visiting Fellow with the Department of Electrical and Computer Engineering, National University of Singapore. He was an Associate Professor (Visiting) with the Research Institute of Electronics, Shizuoka University, Japan. He is currently an Associate Professor with the School of Mines and Metallurgy, Kazi Nazrul University, West Bengal, India, where he has been actively engaged in teaching, research, and administration. He has 53 technical articles in different journals and 55 conference proceedings, eight authored books, 18 edited volumes, and ten book chapters of international repute. He has received research grants from different funding agencies, namely, SERB, DST-ASEAN, DST-JSPS, and UGC. He has also received international research grant from the Centre of Biomedical Engineering, Tokyo Medical and Dental University, in association with RIE, Shizuoka University, Japan, for four consecutive years, from 2019 to 2023. He has supervised six Ph.D. students to date. His research interests include carrier transport in low dimensional systems and electronic devices, nonlinear optical communication, THz semiconductor source, the IoT, and optimization. He is a Life Member of the Institute of Engineers, India, MGMI, and a regular fellow of the Optical Society of India. He was a reviewer for reputed journals. He was selected for the IE (I) Young Engineer Award, from 2019 to 2020, the KNU Best Researcher Award (Engineering and Technology), in 2021, the KNU Best Faculty Award, in 2022 (Faculty of Science and Technology), and the best paper award in different international conferences. He has organized and chaired different international conferences in India and abroad.

SAURAV MALLIK (Member, IEEE) received the Ph.D. degree from the Department of Computer Science and Engineering, Jadavpur University, Kolkata, India, in 2017. His Ph.D. works were conducted with the Machine Intelligence Unit, Indian Statistical Institute, Kolkata, India. He is currently a Research Scientist with The University of Arizona, USA. Previously, he was a Postdoctoral Fellow in environmental epigenetics with the Harvard T. H. Chan School of Public Health, University of Texas Health Science Center at Houston, and University of Miami Miller School of Medicine, USA. He has co-authored more than 156 research articles with a Google H-index of 22. His research interests include computational biology, bioinformatics, data mining, biostatistics, pattern recognition, machine learning, soft computing, and electronics and communications. He was a recipient of the Research Associate of the Council of Scientific and Industrial Research, MHRD, Government of India, in 2017. He was also a recipient of the Emerging Researcher in Bioinformatics Award from the Bioclues, BIRD Award Steering Committee, India, in 2020. He is an editor of many journals.

NAIM AHMAD received the M.S. degree in computer and information sciences and the Ph.D. in enterprise systems from the University of South Alabama, Mobile, USA. He worked in the USA as a Research Assistant with U.S. DOE funded project and as a Graduate Assistant. He has taught as an Assistant Professor with the Management and Engineering Colleges, India, for seven years. He has been a Faculty Member of King Khalid University, Saudi Arabia, since 2013. He has publications in refereed international journals, conferences, and book chapters. His current research interests include enterprise systems, E-learning, sustainability, data science, and MCDM. He received the Upsilon Pi Epsilon Award for Computing Excellence, in 2003, at USA.

WADE GHRIBI received the Ph.D. degree in computer engineering from Kharkiv National University of Radio Electronics, Kharkiv, Ukraine. He is currently an Assistant Professor with the Department of Computer Engineering, College of Computer Science, King Khalid University, Abha, Saudi Arabia. He is in teaching profession for more than 14 years. He has presented 25 papers in national and international journals, conference, and symposiums. His research interests include hardware fault free simulation for SOC, artificial intelligence, and machine learning.